Electronic Supplementary Material (ESI) for Journal of Materials Chemistry A.

Support Information

Miscibility Driven Morphology Modulation in Ternary Solar Cells

Ting Yu,[a] Francesco Tintori,[b] Yuchen Zhang,[c] Wanting He,[a] Edward Cieplechowicz,[b] Raja Sekhar Bobba,[c] Poojan Indrajeet Kaswekar,[c] Maziar Jafari,[d] Yuxuan Che,[e] Yong Wang,[a] Mohamed Siaj,[d] Ricardo Izquierdo,[f] Dmytro F. Perepichka,[e] Quinn Qiao,[c] Gregory C. Welch[b]* and Dongling Ma[a]*

[a] *Énergie, Matériaux et Télécommunications, Institut National de la Recherche Scientifique (INRS), 1650 Boul. Lionel-Boulet, Varennes, Québec, Canada, J3X 1P7*

[b] *Department of Chemistry, University of Calgary, 2500 University Drive N. W., Calgary, Alberta, Canada, T2N 1N4*

[c] *Department of Mechanical and Aerospace Engineering, Syracuse University, NY 13244, USA.*

[d] *Département de chimie, Université du québec à montréal, 405 Rue Sainte-Catherine Est, Montréal, Québec, Canada, H2L 2C4*

[e] *Department of Chemistry, McGill University, Montreal, Quebec, Canada, H3A 0B8*

[f] *Département de génie électrique, École de technologie supérieure, Montréal, Québec, Canada, H3C 1K3*

Materials and Methods

Materials: All starting materials and solvents were purchased from Millipore Sigma, unless indicated otherwise. SiliaCat® DPP-Pd heterogeneous catalyst was purchased from silicycle. All chemicals were used without further purification. Poly[[4,8-bis[5-(2-ethylhexyl)-2-thienyl]benzo[1,2-*b*:4,5-*b′*]dithiophene-2,6-diyl]-2,5-thiophenediyl[5,7-bis(2-ethylhexyl)-4,8-dioxo-4*H*,8*H*-benzo[1,2-*c*:4,5-*c′*]dithiophene-1,3-diyl]] (PBDB-T) polymer and 9-Bis(2-methylene-((3-(1,1-dicyanomethylene)-6,7-difluoro)-indanone))-5,5,11,11-tetrakis(4-hexylphenyl)-dithieno[2,3-d:2',3'-d']-s-indaceno[1,2-*b*:5,6-*b*']dithiophene (ITIC-4F) were purchased from 1-Material company (Canada). Patterned ITO-coated glass substrates (Rs ≤ 10 Ω square^{-1}, Tr ≥ 83%) was bought from Shenzhen Huayu Union Technology Co., Ltd. (China). In addition, zinc acetate dihydrate ($Zn(CH_3COO)_2 \cdot 2H_2O$, 99.9%), ethanolamine ($NH_2CH_2CH_2OH$, 99.5%), 2-methoxyethanol ($CH_3OCH_2CH_2OH$, 99.8%), chlorobenzene (CB) and molybdenum trioxide interlayer (MoO_3) were obtained from Sigma-Aldrich without further purification.

Materials Characterization:

Nuclear Magnetic Resonance (NMR): ^{1}H and ^{13}C NMR spectra were recorded on Bruker Ascend 500 MHz in solvents as indicated. Chemical shifts (δ) are given in ppm. The residual solvent signals were used as references and the chemical shifts converted to the Tetramethylsilane scale (deuterated chloroform ($CDCl_3$): δH = 7.26 ppm, δC = 77.16 ppm).

Cyclic Voltammetry (CV): The instrument used for the electrochemical measurements was a CH instrument 620E potentiostat. The instrument used a standard three-electrode configuration: Ag wire pseudo-reference electrode, Pt wire counter electrode, and glassy carbon working electrode. Experiments were performed in anhydrous dichloromethane (CH_2Cl_2), which was further degassed with a N_2 gas spurge for 10 minutes. Tetrabutylammonium hexafluorophosphate ($TBAPF_6$) was used as the supporting electrolyte. CV sample concentration was ~0.4 mg/mL. The ionization potentials (IP) and electron affinities (EA) were estimated by correlating the onsets of ferrocene (Fc)/Fc^+ redox couple ($E_{ox}^{Fc/Fc+}$, $E_{red}^{Fc/Fc+}$) to the normal hydrogen electrode (NHE), assuming the IP of Fc/Fc^+ redox couple to be 4.80 eV. [1]

$$E(IP) = (E_{ox}+4.80),\ E(EA) = (E_{red}+4.80)$$

Devices Fabrication and Characterization

An inverted structure of ternary organic solar cells (indium tin oxides (ITO) glass/zinc oxide (ZnO)/active layer/MoO_3/Ag) was fabricated. ZnO precursor solution was prepared according to a reported procedure.[2] The patterned ITO glass substrates were cleaned by sequential ultrasonication in detergent, deionized water, acetone, and isopropanol, then, dried by the high-pressure nitrogen stream and followed by treatment with

plasma for 10 min. ZnO precursor solution was spin-coated onto the ITO substrate at 4500 rpm for 60 s and then baked in dried air at 200 °C for 1h to form a thin ZnO layer. Then, the PBDB-T/ITIC-4F binary blend and ternary solution containing 10%, 20% and 50% PDI-EH were spin-coated onto the above substrate in the glovebox at the optimized spin-speed of 3000 rpm for 60 s without thermal-annealing to form the active layer. The optimized concentration was 20 mg mL^{-1} with D/A ratio of 1:1 (w/w) (adding 0.5 v% 1,8-diiodooctane (DIO)). Finally, MoO_3 (25 nm) and silver (Ag, 100 nm) were deposited onto the surface of the active layer in an evaporation chamber under a high vacuum of 1×10^{-6} mbar). The effective device area was 0.06 cm^2. The current density versus voltage (*J-V*) characterization was measured by using a class ABA LED solar simulator under AM 1.5G (100 mW cm^{-2}), which was calibrated using a standard KG5 filtered silicon solar cells. The external quantum efficiency (EQE) measurement was conducted on an IQE200B system (Newport Corporation) in a high purity nitrogen-filled glovebox.

Instruments and Characterizations

The UV-visible absorption spectra were obtained on a Cary 5000 UV-vis-NIR spectrophotometer (Varian).

Atomic force microscopy (AFM) measurements were performed on Bruker MultiMode & AFM in the ScanAsyst mode to acquire the topography and phase images of neat and blend films.

Differential scanning calorimetry (DSC) measurements were carried out on DSC 6000 instrument with a temperature range from 30 °C to 360 °C under the nitrogen stream with a heating rate of 10 °C /min. Baseline and temperature were calibrated with Indium and Zinc. The neat materials and blends were prepared from the evaporation of their CB solutions, and the solidified films were thermally annealed in the same conditions as the OSC devices.

Contact angle measurements were performed on a contact angle analyzer equiped with an AM211 Dino-Lite camera under the ambient temperature. A deionized water and ethylene glycol droplet of 6 μL volume was placed on the dry surface. The surface tension values of films were calculated using the Owens-Wendt model [2, 3]:

$$\gamma_L(1 + \cos\theta) = 2\sqrt{\gamma_s^d \gamma_L^d} + 2\sqrt{\gamma_s^p \gamma_L^p}$$

where γ_s^d and γ_L^d refer to dispersion tension of plane surface and liquid, γ_s^p and γ_L^p refer to polar components of the surface energy of plane surface and liquid, while γ_L refers to total tension of liquid.

Two-dimensional grazing incidence wide-angle X-ray scattering (GIWAXS) measurement was carried out at Xeuss 3.0 instrument of the Suzhou vacuum interconnected nanotech workstation using incident X-ray

with a wavelength of 1.34 Å. The 2D-GIWAXS patterns were treated by MATLAB-GIXSGUI software, and 1D out-of-plane (OOP) and in-plane (IP) curves were analyzed by using the Fit 2D software.

The photo-induced force microscopy (PiFM) images and IR spectra were tested on a VistaScope-infrared (IR) microscope from Molecular Vista, Inc, using PtIr-coated silicon cantilevers (PtIr-NCHR) from Nanosensors. The microscope was operated in dynamic mode using the first mechanical mode of the cantilever to detect the PiFM and the second mechanical mode to detect the topography of the sample. The IR source used to excite the sample was manufactured from Block Engineering at the tunable range of 770 cm^{-1} to 1950 cm^{-1}. Spectral acquisition time was 30 seconds for the presented spectra. All spectra have been normalized against the power profile of the laser.

The electron and hole mobility were measured by using the method of space-charge limited current (SCLC) for electron-only devices with the configuration of ITO/ZnO/active layer/LiF/Al and hole-only devices with the configuration of ITO/PEDOT:PSS/active layer/MoO_3/Ag. [4, 5] The charge carrier mobility was determined by fitting the dark current to the model of a single carrier SCLC according to the equation: $J = 9\varepsilon_0\varepsilon_r\mu V^2/8d^3$, where J is the current density, d is the film thickness of the active layer, μ is the charge carrier mobility, ε_r is the relative dielectric constant of the transport medium, and ε_0 is the permittivity of free space. $V = V_{app} - V_{bi}$, where V_{app} is the applied voltage, V_{bi} is the offset voltage. The carrier mobility can be calculated from the slope of the $J^{0.5} \sim V$ curves.

Transient photo-response atomic force microscopy (TP-AFM) mounted on the conductive AFM (Agilent 5500) was conducted to measure local transient photovoltage (TPV) and transient photocurrent (TPC) decays at different locations on the donor-acceptor blend by using the contact mode. The green laser (MGL-I-532 DPSS; 532 nm) was illuminated from the bottom of ITO glass. A budget sensor (platinum/ chromium coated silicon conductive tip) was used in this measurement. A breakout box (Agilent N9447A) was connected to the oscilloscope (Agilent MSOX4154A) to receive the transient signal from the AFM.

Synthetic Details

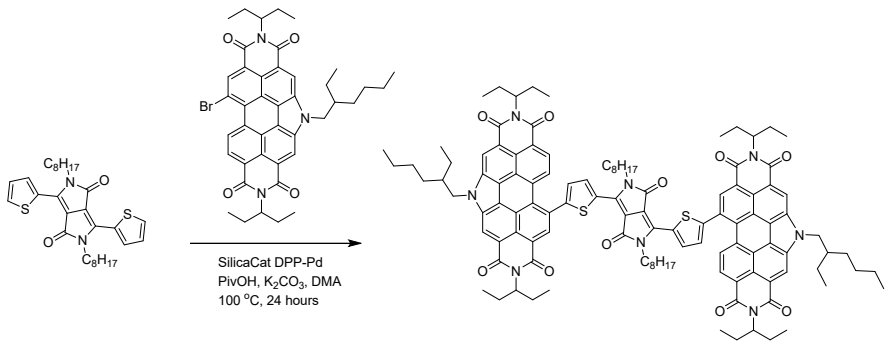

Scheme S1. The synthetic route of PDI-EH molecule.

Synthetic Details of PDI-EH: Reactions were carried out on a bench top or under an atmosphere of dry, nitrogen (N_2) where indicated. For reactions requiring heat, the conventional method involved submerging reaction vial/round bottom flask in a LabArmor® bead bath and heating on a hot plate at the desired temperature was used.

Synthesis of PDI-EH: In a 20 mL microwave vial 2,5-bis(1-octyl)-3,6-di(thiophen-2-yl)diketopyrrolopyrrole (76 mg, 1 eq.), 11-bromo-5-ethylhexyl-2,8-bis(1-ethylpropyl)perylene diimide (234 mg, 2.2 eq.), Silia*Cat*® DPP-Pd (29 mg, 5 mol %), pivalic acid (5 mg, 30 mol %) and cesium carbonate (120 mg, 2.5 eq.) were added with a stir bar and sealed with a crimp sealed septa cap. The contents were purged with N_2 gas followed by the addition of degassed anhydrous *N, N'*-dimethylacetamide (5.3 mL) via syringe. The reaction mixture was heated at 100 °C in a LabArmor® beads bath for 24 hours. After 24 hours the reaction mixture was poured into acetone and allowed to stir for one hour. The precipitated product was collected by filtration and the filtrate was discarded. The solid product was subsequently washed with dichloromethane to solubilize, and isolate it from the insoluble silica-supported catalyst using a silica gel plug. The filtrate was concentrated by rotary evaporation and solubilized in a minimal amount of $CHCl_3$. EtOAc was added dropwise over several hours to the $CHCl_3$ solution and allowed to stir overnight. The precipitated product was isolated by filtration. This yielded a dark solid product (186 mg, 70 % yield). **^{1}H NMR (500 MHz, $CDCl_3$):** δ 9.38 (d, *J* = 3.9 Hz, 1H), 9.10 (s, 1H), 9.05 (s, 1H), 8.89 (s, 1H), 8.62 (s, 1H), 8.34 (d, *J* = 8.3 Hz, 1H), 7.63 (d, *J* = 3.9 Hz, 1H), 5.28 – 5.14 (m, 2H), 4.88 – 4.78 (m, 2H), 4.21 – 4.14 (m, 2H), 2.45 – 2.27 (m, 5H), 2.05 – 1.94 (m, 4H), 1.87 (dt, *J* = 15.5, 7.9 Hz, 2H), 1.55 – 1.32 (m, 8H), 1.34 – 1.24 (m, 5H), 1.22 – 1.15 (m, 2H), 1.15 – 1.07 (m, 4H), 0.98 (ddd, *J* = 18.2, 11.2, 4.6 Hz, 14H), 0.87 (t, *J* = 7.3 Hz, 3H), 0.69 (t, *J* = 6.9 Hz, 3H).

^{13}C NMR (126 MHz, $CDCl_3$): δ 161.57, 147.90, 139.82, 137.18, 135.52, 132.64, 132.00, 129.06, 128.22, 125.13, 125.02, 123.22, 123.16, 119.94, 119.85, 108.77, 58.06, 51.15, 42.69, 41.78, 31.78, 31.03, 30.31, 29.26, 28.75, 27.04, 25.35, 24.49, 23.17, 22.64, 14.12, 14.11, 11.56, 10.87. 34/57 carbon peaks obtained, quaternary carbons could not all be obtained.

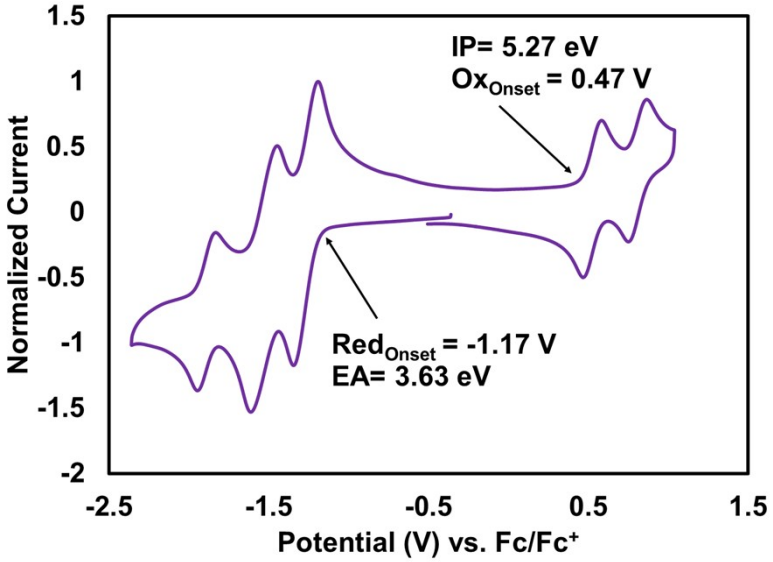

Fig. S1. Cyclic voltammetry curve of PDI-EH, which shows the onsets of oxidation (Ox_{Onset}) and reduction (Red_{Onset}), ionization potentials (IP) and electron affinities (EA), respectively.

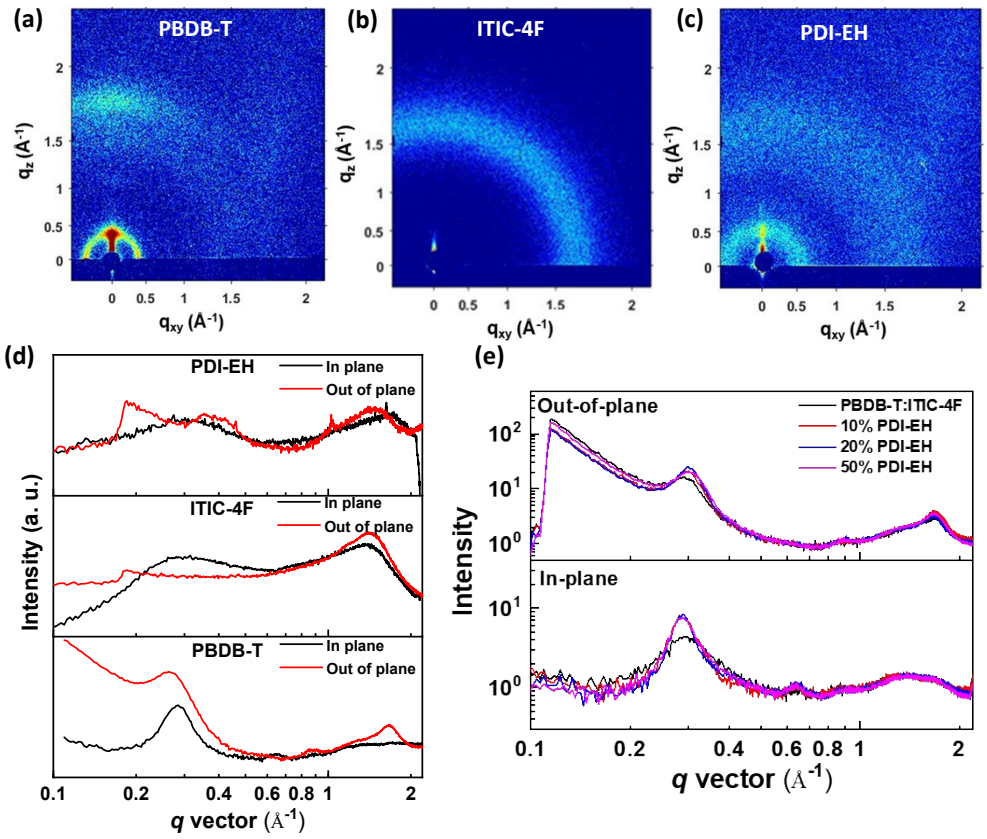

Fig. S2. (a-c) 2D GIWAXS patterns of the pristine PBDB-T, ITIC-4F and PDI-EH films; (d) the out-of-plane and in-plane curves of pristine films related to 2D-GIWAXS patterns; (e) the out-of-plane and in-plane curves of the binary film and ternary films containing 10%, 20% and 50% PDI-EH.

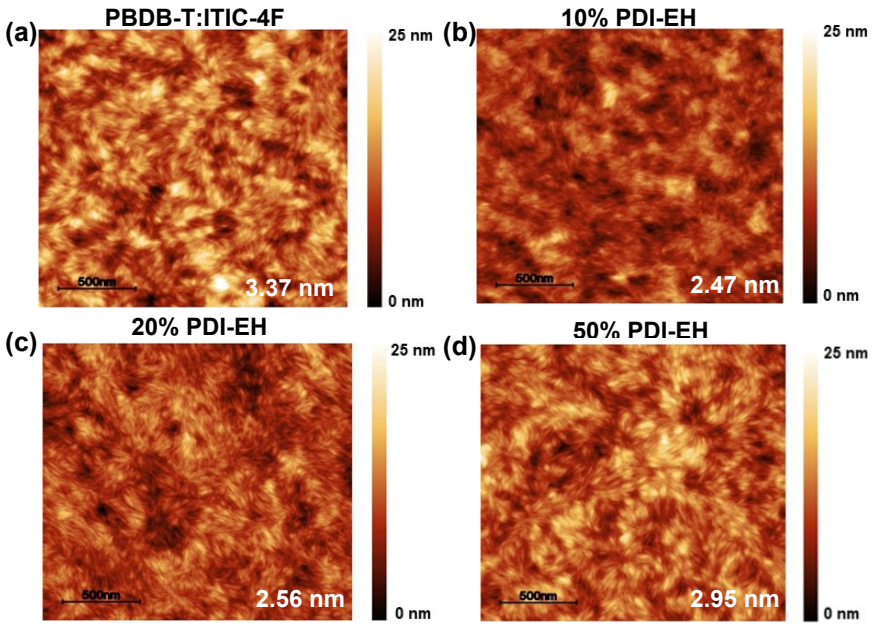

Fig. S3. AFM topography images of PBDB-T/ITIC-4F blend film (a) and ternary blend films containing 10%, 20% and 50% PDI-EH (b-d), AFM images size: 2 um × 2 um. The numbers inside of topography images denote the average RMS roughness value.

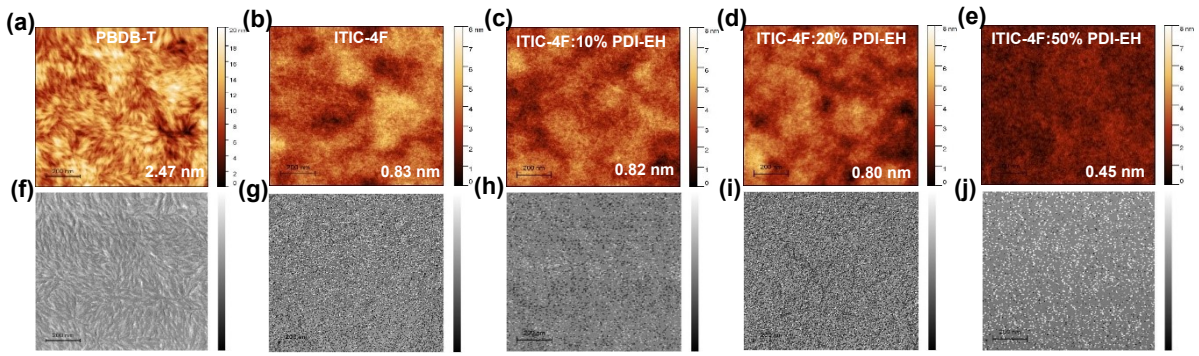

Fig. S4. AFM topography images (a-e) and phase images (f-j) of pristine PBDB-T film (a, f), pristine ITIC-4F film (b, g), ITIC-4F/10% PDI-EH blend film (c, h), ITIC-4F/20% PDI-EH blend film (d, i), and ITIC-4F/50% PDI-EH blend film (e, j). AFM images size: 1 um × 1 um. The numbers inside (a-e) denote the average RMS roughness value.

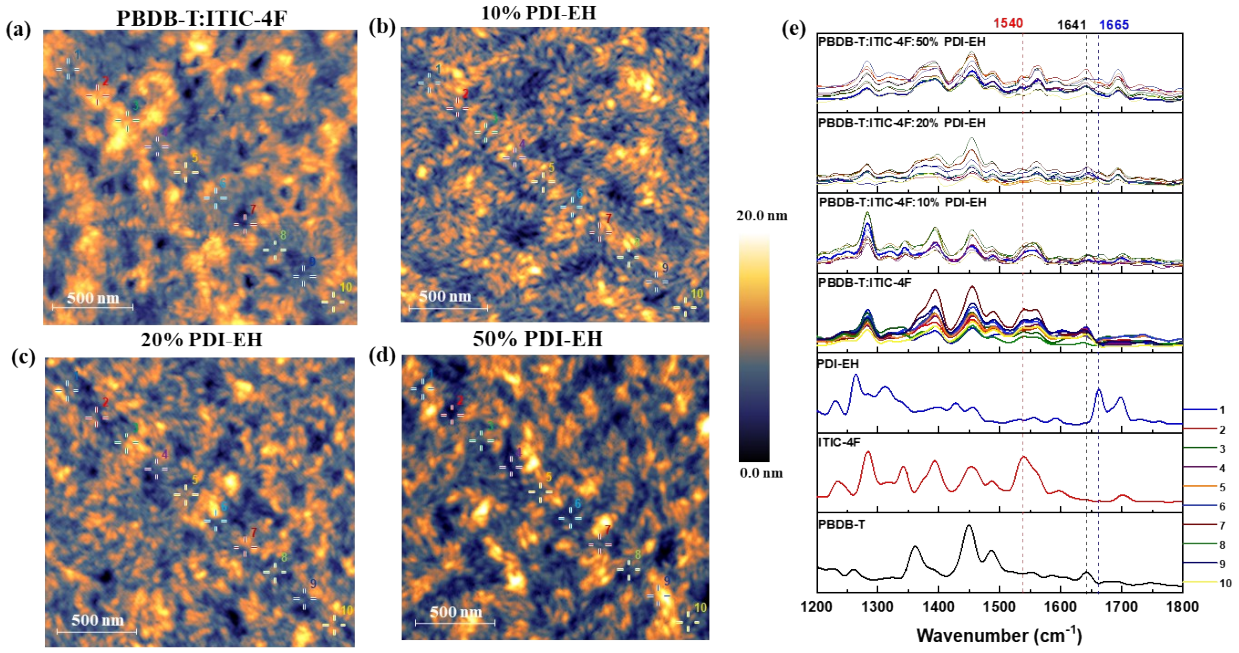

Fig. S5. PiFM topography images of PBDB-T/ITIC-4F blend film (a) and ternary blend films containing 10%, 20% and 50% PDI-EH (b-d); (e) PiFM spectra of the binary film and ternary films containing 10%, 20% and 50%PDI-EH taken from 10 locations as marked in corresponding images. For comparison, PiFM spectra of pristine PBDB-T, ITIC-4F, PDI-EH films are also shown. Topography image size: 2 μm × 2 μm.

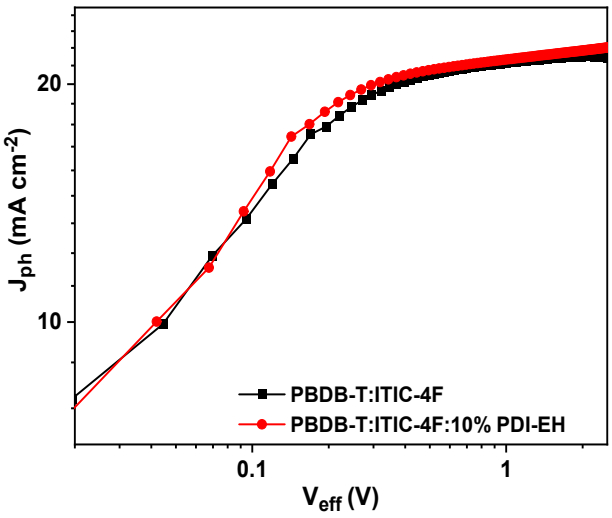

Fig. S6. The J_{ph}-V_{eff} plots for binary blend film and ternary blend films containing 10% PDI-EH.

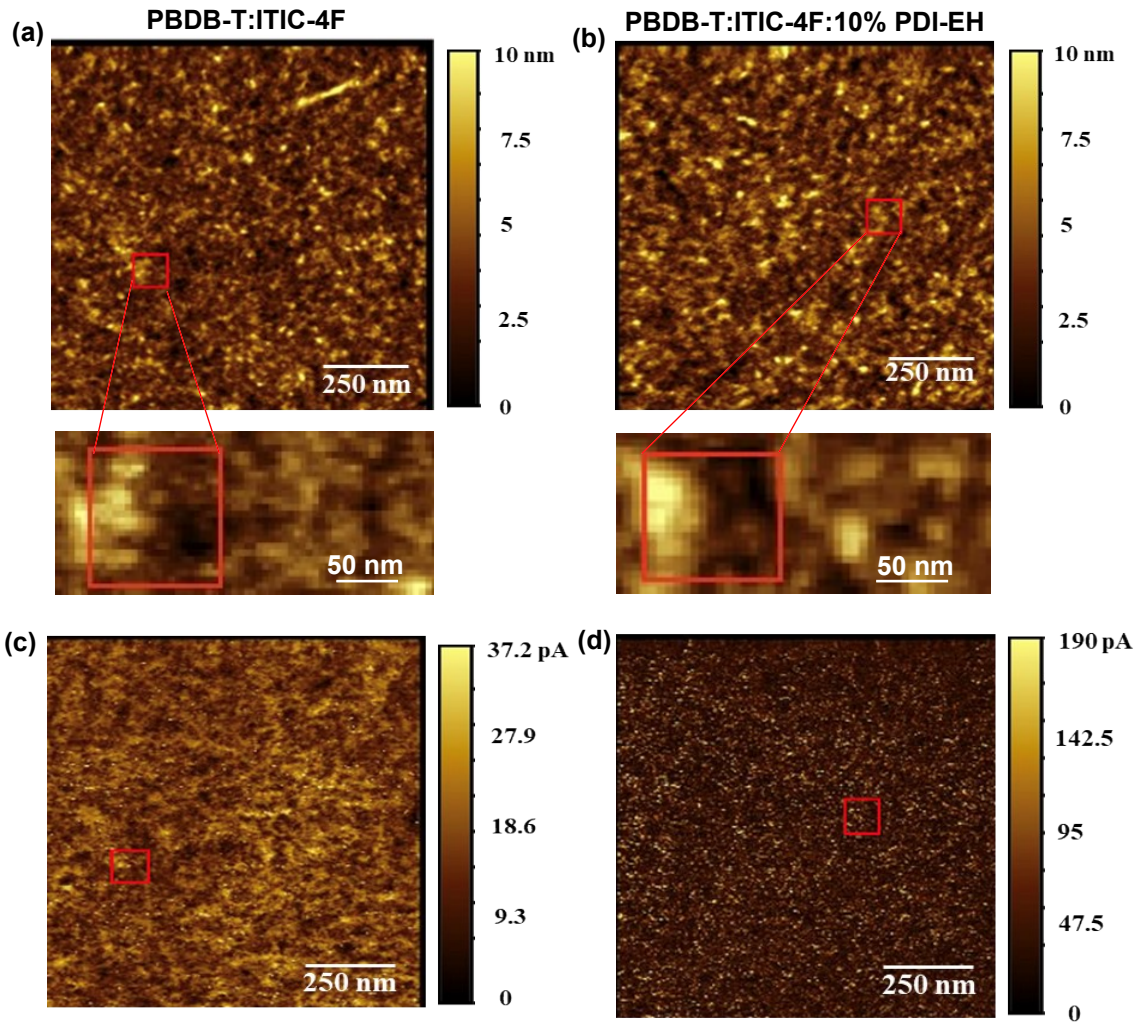

Fig. S7. Topography AFM images of the PBDB-T/ITIC-4F binary film (a) and the 10% PDI-EH-containing ternary film (b); current sensing AFM images of the PBDB-T/ITIC-4F binary film (c) and the 10% PDI-EH-containing ternary film (d). Red rectangles (100 × 100 nm) marked in AFM images were used for nanoscale mappings of τ_r, τ_t and L_D.

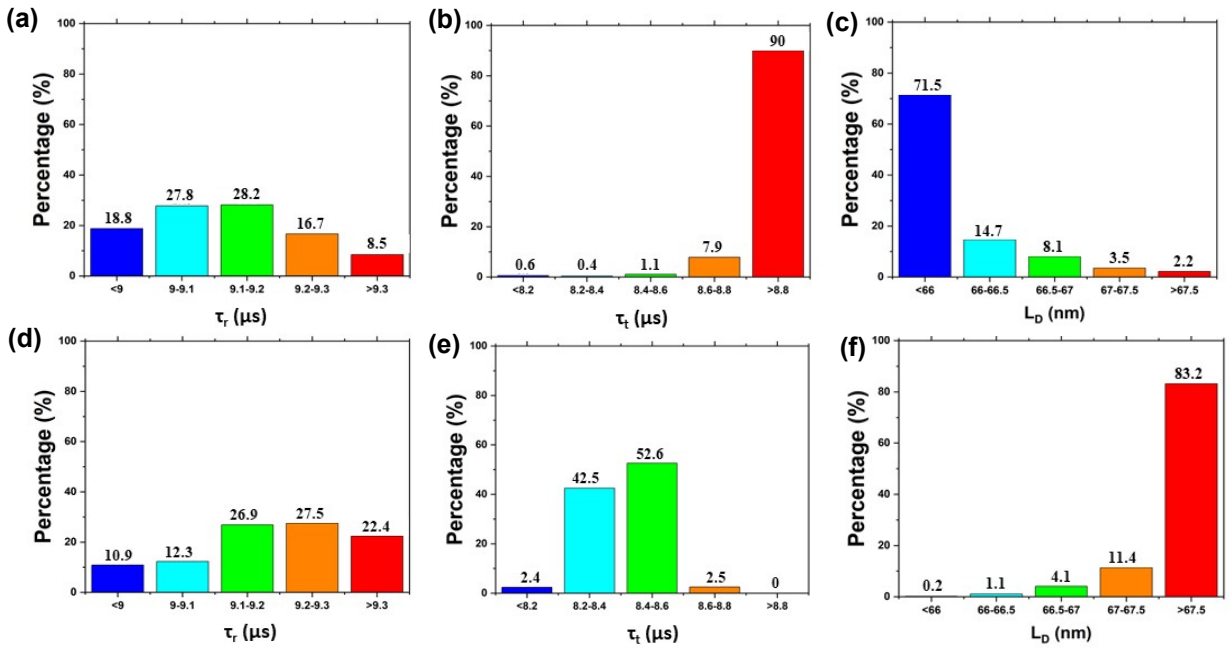

Fig. S8. Histogram distribution of τ_r for (a) PBDB-T/ITIC-4F film and (d)10% PDI-EH-containing ternary film, τ_t for (b) PBDB-T/ITIC-4F film and (e) 10% PDI-EH-containing ternary film, and L_D for (c) PBDB-T/ITIC-4F film and (f) 10% PDI-EH-containing ternary film.

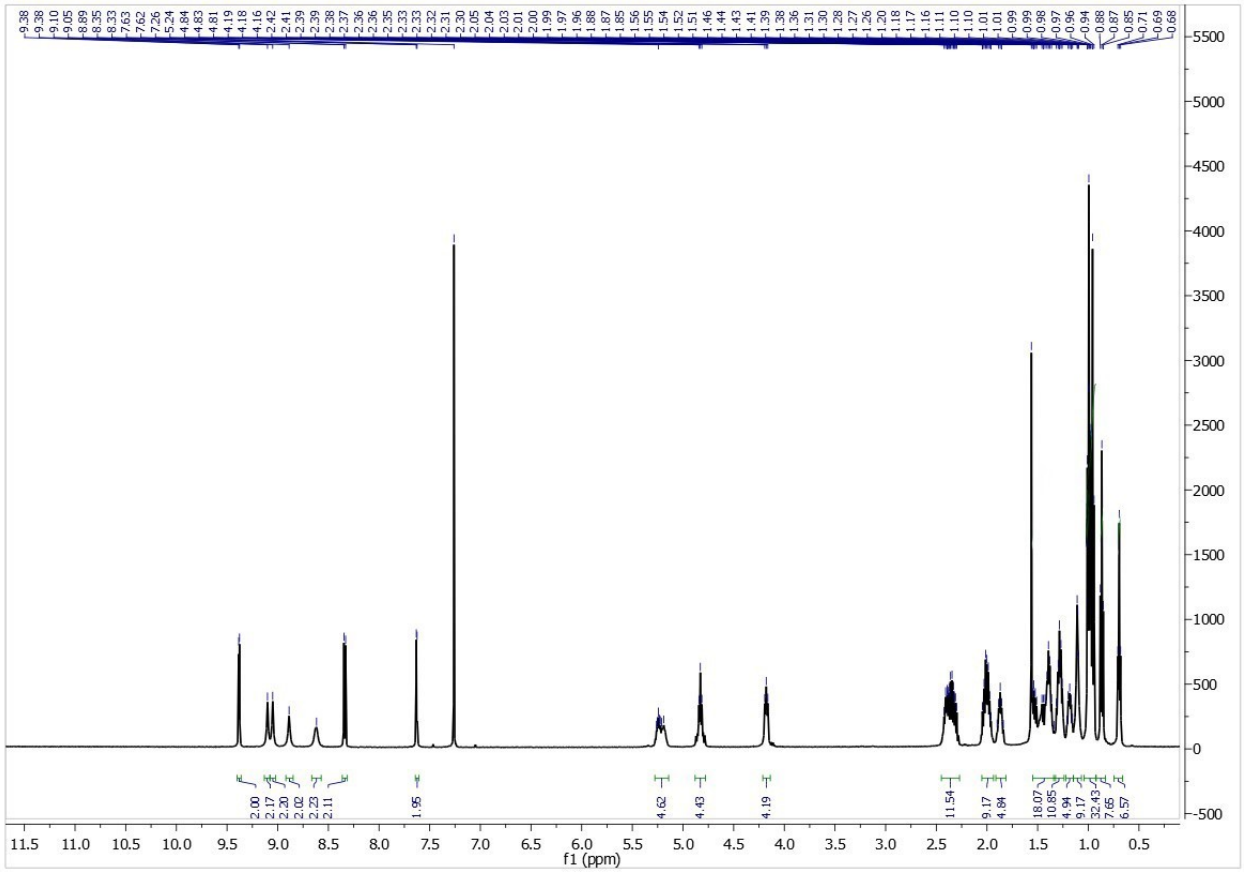

Fig. S9. ^{1}H NMR spectrum of PDI-EH in $CDCl_3$ solution.

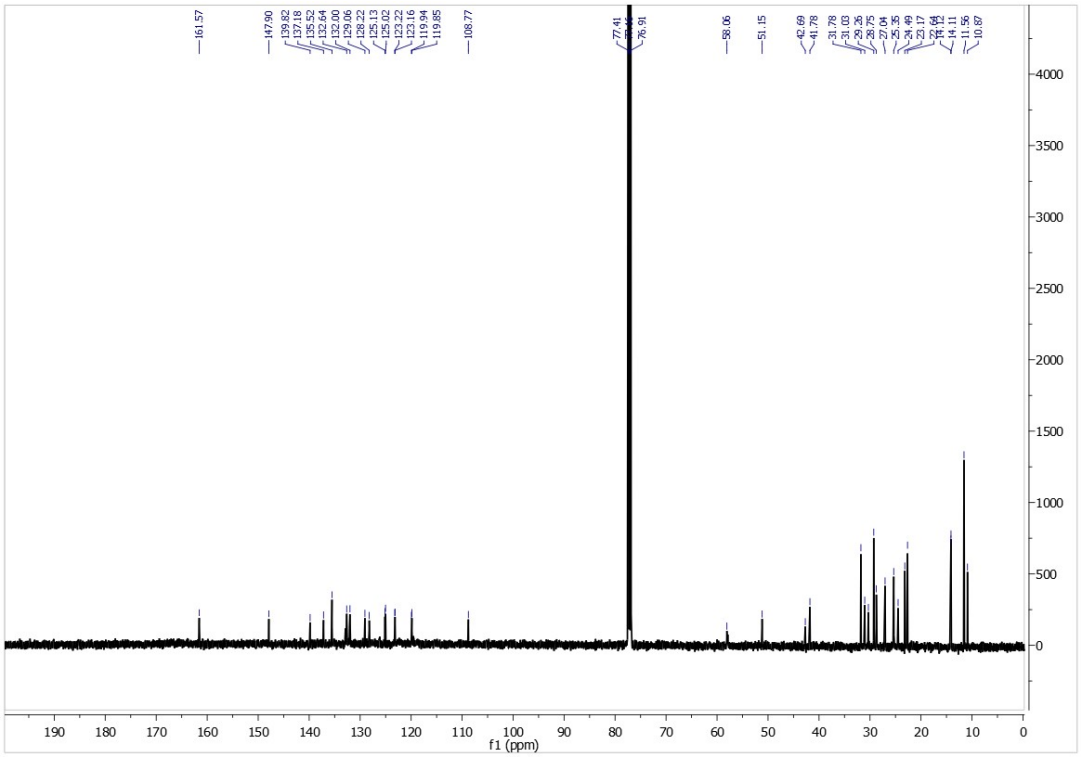

Fig. S10. ^{13}C NMR spectrum of PDI-EH molecule in $CDCl_3$ solution.

Supplementary Tables

Table S1. Hole mobility, electron mobility and the ratio of hole/electron mobility values for binary blend film and ternary blend films with different contents of PDI-EH (10%, 20%, and 50%).

Active layer	Hole mobility(μ_h)	Electron mobility(μ_e)	μ_h/μ_e
PBDB-T : ITIC-4F	1.2×10^{-4}	4.1×10^{-5}	3.0
10% PDI-EH	1.6×10^{-4}	5.8×10^{-5}	2.8
20% PDI-EH	1.8×10^{-4}	4.6×10^{-5}	3.8
50% PDI-EH	1.4×10^{-4}	7.4×10^{-6}	18.4

Table S2. Photovoltaic parameters of binary and ternary inverted solar cells under 6500 K LED and 2700 K LED illuminations.

	Active layer	V_{oc} [V]	J_{sc} [uA cm^{-2}]	FF [%]	PCE (max.)[c] [%]
2700 K LED [a]	**PBDB-T : ITIC-4F**	0.51 (0.52 ± 0.013)	97 (93 ± 3.59)	61 (59 ± 2.40)	10.5 (9.7 ± 0.59)
	10% PDI-EH	0.53 (0.53 ± 0.008)	100 (96 ± 4.13)	65 (65± 2.21)	11.4 (11.1 ± 0.41)
	20% PDI-EH	0.59 (0.59 ± 0.004)	99 (95 ± 5.68)	63 (63± 2.26)	12.0 (11.6 ± 0.44)
	50% PDI-EH	0.64 (0.65± 0.005)	73 (70 ± 4.87)	55 (55± 1.76)	8.5 (8.2 ± 0.26)
6500 K LED [b]	**PBDB-T : ITIC-4F**	0.52 (0.51 ± 0.015)	87 (86± 5.32)	65 (63 ± 2.50)	9.9 (9.1 ± 0.67)
	10% PDI-EH	0.55 (0.53 ± 0.014)	90 (87 ± 3.24)	67 (65 ± 1.70)	10.6 (9.7 ± 0.49)
	20% PDI-EH	0.59 (0.59± 0.005)	95 (89 ± 4.33)	63 (63 ± 1.33)	11.5 (10.1 ± 0.48)
	50% PDI-EH	0.64 (0.64± 0.003)	67 (66 ± 3.86)	55 (55 ± 2.01)	7.6 7.5 ± 0.18)

[a.] measured under 2700 K LED of 300 uW/cm^2 power input.

[b.] measured under 6500 K LED of 310 uW/cm^2 power input.

[c.] average values and standard deviation were obtained over 10 devices, which are shown in brackets.

Reference

[1] J. Pommerehne, H. Vestweber, W. Guss, R. F. Mahrt, H. Bässler, M. Porsch, J. Daub, *Adv.Mater.* **1995**, *7*, 551.

[2] D. K. Owens, R. C. Wendt, *J. Appl. Polym. Sci.* **1969**, *13*, 1741.

[3] H. Wang, L. Han, J. Zhou, T. Liu, D. Mo, H. Chen, H. Lai, N. Zheng, Z. Xie, W. Zheng, *CCS Chem.* **2021,** *3*, 2591.

[4] S. Hultmark, S. H. K. Paleti, A. Harillo, S. Marina, F. A. A. Nugroho, Y. Liu, *Adv. Funct. Mater.* **2020**, 3*0*, 2005462.

[5] J. A. Röhr, D. Moia, S. A. Haque, T. Kirchartz, J. Nelson, *J. Condens. Matter Phys.* **2018**, *30*, 105901.